CrystEngComm

Accepted Manuscript

ROYAL SOCIETY OF CHEMISTRY

www.rsc.org/crystengcomm

Cite this: DOI: 10.1039/c0xx00000x

www.rsc.org/xxxxxx

ARTICLE TYPE

Selective morphologies of MgO via nanoconfinement on γ-Al_2O_3 and reduced graphite oxide (rGO): improved CO_2 capture capacity at elevated temperatures

Xiaoxue Zhang[a], Kaipei Qiu[a] , Erkki Levänen[b] , Zheng Xiao Guo[a]*

[a] *Department of Chemistry, University College London, 20 Gordon Street, London WC1H 0AJ, UK*
[b] *Department of Materials Science, Tampere University of Technology, P.O. Box 589, Tampere, Finland*

Two substrates, γ-alumina (γ-Al_2O_3) and reduced graphene oxide (rGO), have been used to confine the formation of magnesium oxide (MgO) crystals, so as to control crystal growth, reduce crystal size, enlarge surface area and thus increase the CO_2 capture capacity at elevated temperatures. Typically, MgO/γ-Al_2O_3 has been synthesized by a facile sol-gel route, and MgO/rGO has been obtained by calcining the hydrothermally grown magnesium hydroxide ($Mg(OH)_2$) on rGO sheets. Distinct morphologies of MgO have been observed through the above two synthesis routes: spherical particles have been formed when using γ-Al_2O_3 as substrates while MgO nanowiskers appear when the loading ratio of precursor is high in rGO supported samples. The effects of substrate on the morphology of the confined MgO and the corresponding CO_2 uptake are discussed in detail for the first time.

Keywords: MgO, reduced graphite oxide (rGO), CO_2 capture, chemical sorbents

Introduction

It is commonly accepted that anthropogenic carbon dioxide (CO_2) emission is the main cause for global climate change[1,2,3] CO_2 capture has been identified as a significant route to reduce CO_2 emission before the complete realization of renewable green energies. Amine scrubbing using aqueous solutions of alkanolamines is the current commercially used technology to capture CO_2 [4]. However, the CO_2 desorption increases the energy cost roughly by 25-40 %, the equipment suffers from corrosion, and treatment of aqueous sorbent adds extra cost and environmental concern of water contamination[4]. Therefore a variety of alternative solid sorbent materials via physisorption and chemisorption are under active development[5,6]. Physisorbents are typically zeolites [7], amine functionalized porous silicas [8], carbons[9], metal-organic frameworks (MOFs)[10], which are porous with well-defined pore structures and high specific surface areas to capture CO_2 molecules while requiring low regeneration energy. However, these sorbents are mainly for CO_2 capture at low temperatures. In addition, zeolites and amine functionalized porous silicas have shown low tolerance to moisture[11], and MOFs generally suffer from a weak stability under hydrolytic condition and furthermore a small production scale. On the other hand, chemical sorbents, such as Li_2O, CaO, MgO, can be used in much higher temperatures to capture CO_2 by forming carbonates[12]. K_2CO_3 and $NaCO_3$ can also capture CO_2 with the presence of water to form hydrogen carbonates[13]. However, in general, these chemical sorbents suffer from two major concerns of high regeneration temperature and low capture capacity.

MgO shows lower regeneration temperatures (at 400-500 °C) than CaO, and is more cost-effective than Li_2O[12]. However the practical capacity of MgO is limited as only the surface reacts with CO_2 and the formed surface carbonate layer largely slows down subsequent reactions. Therefore increasing the active surface area of MgO to allow efficient contact with CO_2 can enhance the CO_2 uptake. Previous research has focused on fabricating mesoporous MgO and the use of pre-designed porous carbon as substrates [1,2,3]. However there is lack of study on the control and the effects of MgO morphology on CO_2 uptake.

In this paper, we proposed two new approaches to control and maximize the surface area of MgO crystals. In one approach, we used a straightforward sol-gel route to obtain MgO/γ-Al_2O_3 composite. In the other, we firstly grew $Mg(OH)_2$ on rGO sheets by a facile hydrothermal method and then obtained MgO by calcining the $Mg(OH)_2$ at 500 °C. The surface areas of MgO were significantly increased in both methods. However the morphologies of MgO obtained were very different, leading to different CO_2 uptake. Therefore this study, for the first time, demonstrates that different crystal structures can be derived from various substrates, which in turn also affects the CO_2 capture capacity.

Experimental Details

Synthesis of MgO/γ-Al_2O_3

MgO/γ-Al_2O_3 was obtained by a simple sol-gel route, which was modified from a previously reported process of forming high surface area γ-alumina[14,15,16]. The raw materials were magnesium acetate tetrahydrate ($Mg(CH_3COO)_2{\cdot}4H_2O$, Sigma-Aldrich),

aluminium tri-sec-butoxide (denoted as $Al(O\text{-}sec\text{-}Bu)_3$, $C_{12}H_{27}AlO_3$ > 97%, Aldrich), 2-propanol (denoted as i-PrOH, C_3H_7OH > 99.5%, Aldrich) and ethyl acetoacetate (denoted as EAcAc, $C_6H_{10}O_3$ > 99%, Sigma-Aldrich). Different molar ratios (1.72:1, 0.86:1, 0.43:1) of $Mg(CH_3COO)_2{\cdot}4H_2O$ to $C_{12}H_{27}AlO_3$ were applied in precursor. In a typical precursor preparation using the molar ratio of 1.72:1, 0.5 g $C_{12}H_{27}AlO_3$, 30 ml i-PrOH and 2 ml EAcAc were mixed and stirred at room temperature for 1 h. Then 2 g $Mg(CH_3COO)_2{\cdot}4H_2O$ was introduced, and the solution was stirred for 1 h. Finally 5 ml distilled water was added for hydrolysis to form a gel. The gel was then dried at 120 °C to form fine powder, which was calcined at 500 °C for 3 h with a heating rate of 2 °C/min in air to form MgO/γ-Al_2O_3. The samples were named as MxAy, where M and A represented MgO and γ-Al_2O_3, x and y indicated the molar ratio of $Mg(CH_3COO)_2{\cdot}4H_2O$ to $Al(O\text{-}sec\text{-}Bu)_3$ in the precursor preparation. Pure MgO and γ-Al_2O_3 was also prepared with the same route as references.

Synthesis of MgO/rGO

Graphene oxide (GO) was synthesized by a modified Hummer method[17]. Different amount (0.1 g, 0.5 g, 1 g) of magnesium nitrate hexahydrate ($Mg(NO_3)_2{\cdot}6H_2O$, Sigma-Aldrich) was dispersed in 20 ml GO aqueous suspension (GO concentration 2 mg/ml) for 1 h. Then ammonia aqueous solution (NH_4OH, 35%, Fisher Scientific) was added to adjust the pH value to 10, and then vigorously stirred for 1 h. The mixture was then placed into the Teflon liner in autoclave, and kept at 180 °C for 12 h to form $Mg(OH)_2$ on GO sheets. Meanwhile the GO was reduced to rGO under the hydrothermal condition[18]. After the hydrothermal process, the mixture was collected and washed with distilled water to remove the excessive OH^- ions using centrifuge. Finally, the products were freeze-dried and then calcined under N_2 at 500 °C for 3 h with a heating rate of 2 °C/min to obtain MgO/rGO. Pure MgO without use of GO in precursor was also prepared with the same processing route as reference. The hydrothermally synthesized samples were named as $Mg(OH)_2$/rGO-x and $Mg(OH)_2$-x, and the calcined samples are named as MgO/rGO-x and MgO-x (x=0.1, 0.5, 1) respectively, where x indicated the weight (g) of magnesium nitrate hexahydrate used in the precursor.

Characterization

Crystalline phase was determined by a powder X-ray diffraction (XRD) pattern (Stoe Stadi-P Capillary PXRD) using Cu Kα radiation. The XRD pattern was measured from a 2θ range of 10° to 90° or 15° to 85° with a step size of 0.5° and a count time of 10 s per step. N_2 adsorption/desorption isotherms were obtained by using a gas sorption experiment (Quantachrome Autosorb iQ-c) at the temperature of liquid nitrogen. The samples were degassed at 200 °C prior to the measurement. The data analysis was carried out with ASiQwin software. The specific surface areas were calculated by the Brunauer-Emmett-Teller (BET) equation using the data in a P/P_0 range of 0.15–0.35. The pore size distribution in range of 2-200 nm was obtained by a Barett-Joyner-Halenda (BJH) model from the desorption branches of the isotherms. The morphology and elemental information of the samples were studied by a high resolution transmission electron microscope (HRTEM, JEM 2100). The Fast Fourier Transform (FFT) analysis of the HRTEM images was carried out by image analysis software, Gatan DigitalMicrograph Suite. The STEM (scanning transmission electron microscopy) mode in the HRTEM was used to analyse the elemental information. The CO_2 capture capacity was obtained via Thermalgravimetric analysis (Setaram Setys 16/18). The samples were firstly kept at 200 °C under Ar to remove all the moistures, and then the temperature was raised to 400 °C where the gas was changed from Ar to CO_2. The increase in weight was utilized to calculate the CO_2 capture amount.

Results and Discussion

Structure of MgO/ γ-Al_2O_3

XRD patterns of the MgO/γ-Al_2O_3 composites are presented in figure 1, where the diffraction peaks were indexed according to MgO (JCPDS card of 75-447). The broad peak around 20° was from the glass capillary sample holder, and the small arrowed peak around 60° was a noise peak which was later identified to be from a bad alignment of the X-ray beam. Pure MgO and γ-Al_2O_3 was processed with the same procedure for comparison by using only $Mg(NO_3)_2{\cdot}6H_2O$ or $C_{12}H_{27}AlO_3$ in the precursor. When increasing the amount of $Mg(NO_3)_2{\cdot}6H_2O$ in precursor, the diffraction peaks of the resulted products shifted closer to the MgO peaks positions. The intensity of the diffraction peaks also got sharper, indicating increased crystallinity and crystal growth.

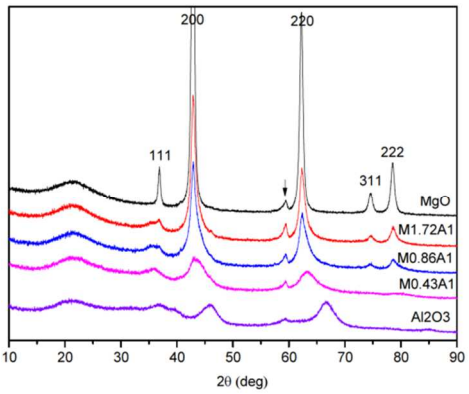

Figure 1. XRD patterns of pure MgO, MgO/γ-Al_2O_3 and pure γ-Al_2O_3 made by sol-gel method.

The specific surface area, N_2 adsorption/desorption isotherms and pore distribution of the pure MgO and MgO/γ-Al_2O_3 composites are shown in figure 2. Use of γ-Al_2O_3 substrate to confine MgO crystals was effective to increase the specific surface area significantly from 80 m^2/g (for pure MgO) to 283 m^2/g (for M0.86A1). All the isotherms were type IV isotherms, which were related to mesoporous structure. M0.43A1 had bimodal pore distribution at 2-3 nm and 20 nm, while M0.86A1 had bimodal pore distribution at 2-3 nm and 30 nm. With the increase of the MgO amount, M1.72A1 and pure MgO had nearly one pore distribution around 20 nm and 5 nm respectively.

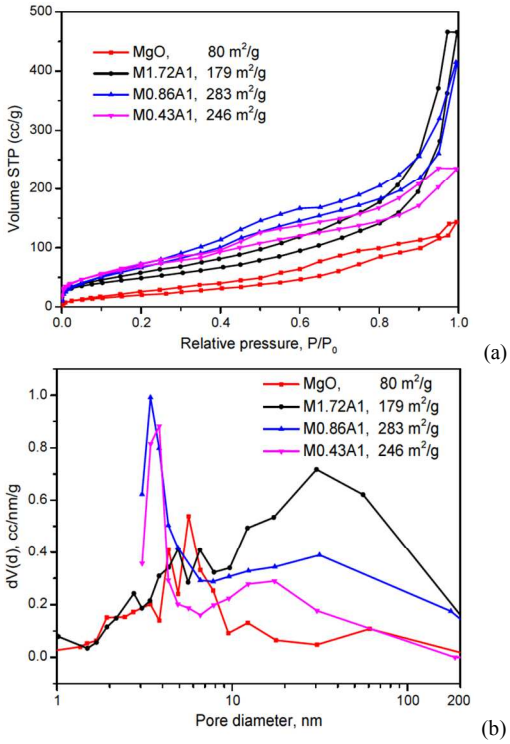

Figure 2. (a) N_2 adsorption/desorption isotherms and (b) pore distribution of MgO and MgO/γ-Al_2O_3 made by sol-gel method.

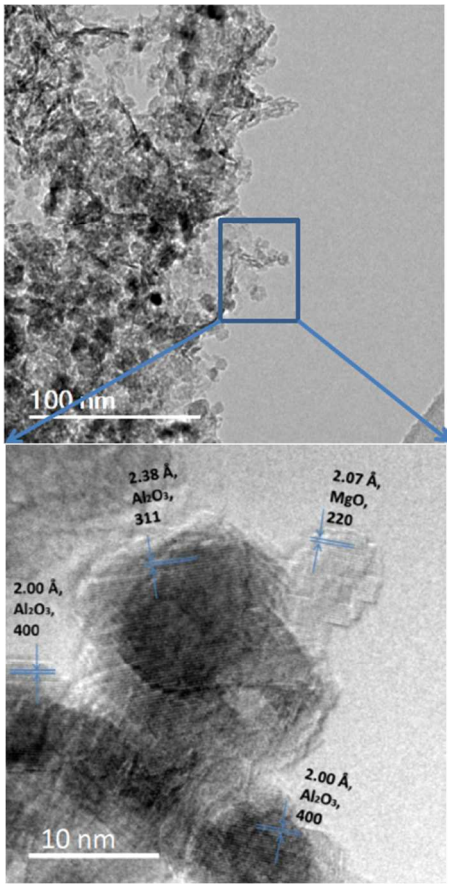

Figure 3. TEM and lattice image of M0.86A1 made by sol-gel method. The lattice fringes are from the squared area and indexed to belong to MgO and γ-Al_2O_3.

The morphology of M0.86A1 having the highest surface area was studied under HRTEM (see figure 3). The product mainly contained spherical particles, which agglomerated together. The squared area was observed further by increasing the magnification to show lattice fringes, which were indexed to be MgO and γ-Al_2O_3. The lattice fringes results confirmed that the crystallites of MgO and γ-Al_2O_3 were mixed together, having crystallites size up to 10 nm in spherical morphology.

Structure of MgO/rGO

Another approach was designed in this study to confine the MgO crystals on 2D layered material of graphene. By use of GO in precursor, $Mg(OH)_2$ can form bonding with GO to effectively confine MgO onto the 2D sheets. Figure 4 (a) gives the XRD patterns of $Mg(OH)_2$ obtained with and without GO in precursor. All the diffraction peaks belonged to $Mg(OH)_2$, according to the JCPDS card 83-114. The $Mg(OH)_2$ grown on GO sheets had much lower peak intensity, indicating smaller particle size due to the confined growth on the rGO sheets. Besides when using GO in precursor, the peak intensity of $Mg(OH)_2$/rGO-1 was rather same with that of $Mg(OH)_2$/rGO-0.5, though the amount of $Mg(NO_3)_2$ was doubled in precursor. However, without using GO in precursor the peak intensity of $Mg(OH)_2$-1 was much higher than that of $Mg(OH)_2$-0.5, indicating a much larger crystal size in $Mg(OH)_2$-1. After calcining at 500 °C, the $Mg(OH)_2$ transformed to MgO, as shown in figure 4 (b). Again the pure MgO produced had much higher peak intensity that that of MgO on rGO, resulted from its much larger crystal size.

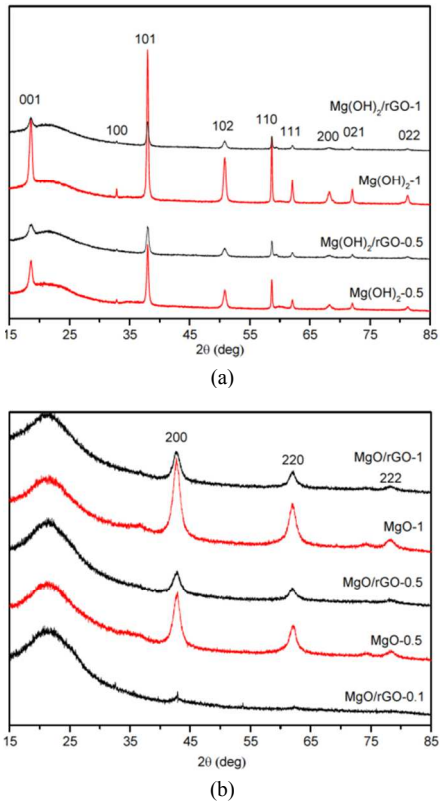

Figure 4. XRD patterns of $Mg(OH)_2$-x and $Mg(OH)_2$/rGO-x in (a), and MgO-x and MgO/rGO-x in (b). x=0.5 and 1.

The specific surface area, N_2 adsorption/desorption isotherms, and pore distribution of the MgO/rGO samples are shown in figure 5, as compared with the MgO produced without use of GO in precursor. In both cases, use of GO were successful to increase the specific surface area, and MgO/rGO-0.5 had the highest surface area of 191 m^2/g. The pore distributions of MgO-x and MgO/rGO-x samples are shown in figure 5 (b), where there was more pore distributed around 100 nm when using GO in precursor.

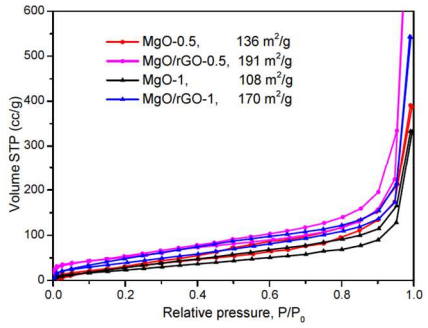

(a)

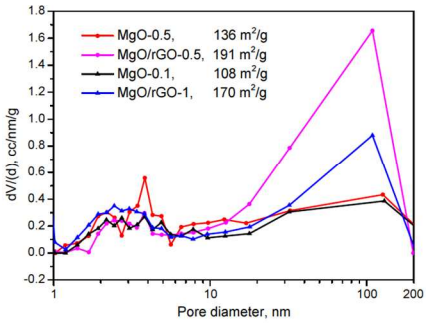

(b)

Figure 5. N_2 adsorption/desorption isotherms (a) and pore distribution (b) of MgO-x and MgO/rGO-x. x=0.5 and 1.

The morphology of MgO obtained on rGO is very different with the ones confined on γ-Al_2O_3. Figure 6 (a) shows the morphology of $Mg(OH)_2$-1 without use of GO in precursor. The crystals were in size of 100 - 300 nm, having hexagonal and spherical shape, as $Mg(OH)_2$ has hexagonal lattice. After calcining, the crystals maintained similar morphology and size, as shown in figure 6 (b). However, use of GO substrate changed significantly the morphology of the resulted MgO. For MgO/rGO-1, the rGO sheets were covered with MgO crystals, and large amount of nanowhiskers were also observed, as shown in figure 6 (c). After increasing the magnification, it was found that some of the nanowhiskers were actually double layer packed, with empty interval between the two layers. To our best knowledge, such morphology was not reported for MgO in literature. The lattice fringes of the squared area in (d) is shown in (e) with its corresponding FFT inserted and indexed to be MgO with beam direction of [011], confirming that rGO sheets were covered with MgO crystals. In order to confirm the nanowhiskers were from MgO, STEM was carried out. The image under STEM mode is generally much more blurred than in the HRTEM mode, which makes it difficult to check the elemental information for small particles. However, we were able to relate our STEM image to the HRTEM image from the same area, as shown in (e). The elemental scanning was carried out in the red circled area where the whisker pointed out without any sheets under it. The red dots in the STEM image represented the distribution of Mg element, proving that the nanowhiskers were made of MgO.

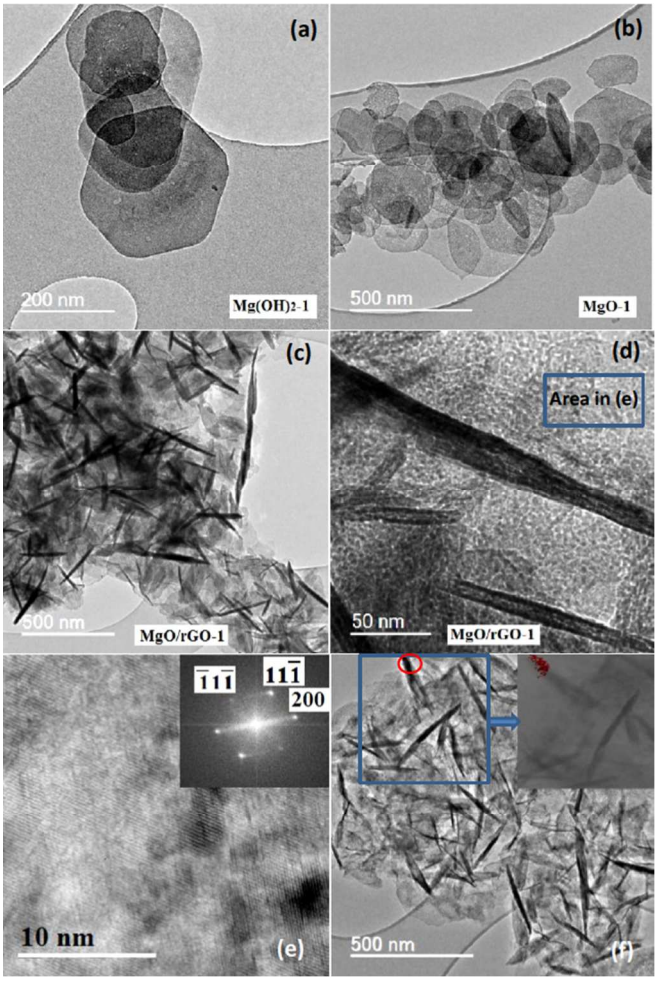

Figure 6. TEM images of $Mg(OH)_2$-1 in (a) and the calcined MgO-1 in (b). The morphologies of MgO/rGO-1 are shown in (c,d), with its lattice fringes and FFT pattern in (e) and STEM elemental analysis in (f). The FFT inserted is from the whole area in (e) the beam direction is indexed to be [011].

The calculated MgO weight in MgO/rGO-1was 172 mg, while GO used was 40 mg. Therefore we speculated that in this sample, MgO could not fully accommodate onto the rGO sheets. Without the confinement on the 2D rGO layers, MgO nanowhiskers were therefore formed following a crystal growth along z axis for hexagonal lattice.

In order to confirm this speculation, we therefore deceased the amount of $Mg(NO_3)_2$ in precursor to 0.5 g, and obtained MgO-0.5 and MgO/rGO-0.5. For MgO-0.5, the particles are in spherical and hexagonal shapes (figure 7a), same as in MgO-1. While for MgO/rGO-0.5, we also observed nanowhiskers however with a much less amount in figure 7b due to the decease of $Mg(NO_3)_2$ in precursor. Uncovered graphene edges were also observed, as shown in figure 7c. Meanwhile, we again found the double layer packed morphology, see figure 7d. We further decreased the

amount of $Mg(NO_3)_2$ in precursor to 0.1 g to have much less amount of MgO than GO. As expected, the MgO crystals were only formed on the rGO sheets and no whiskers were observed, as shown in figure 7 (e).

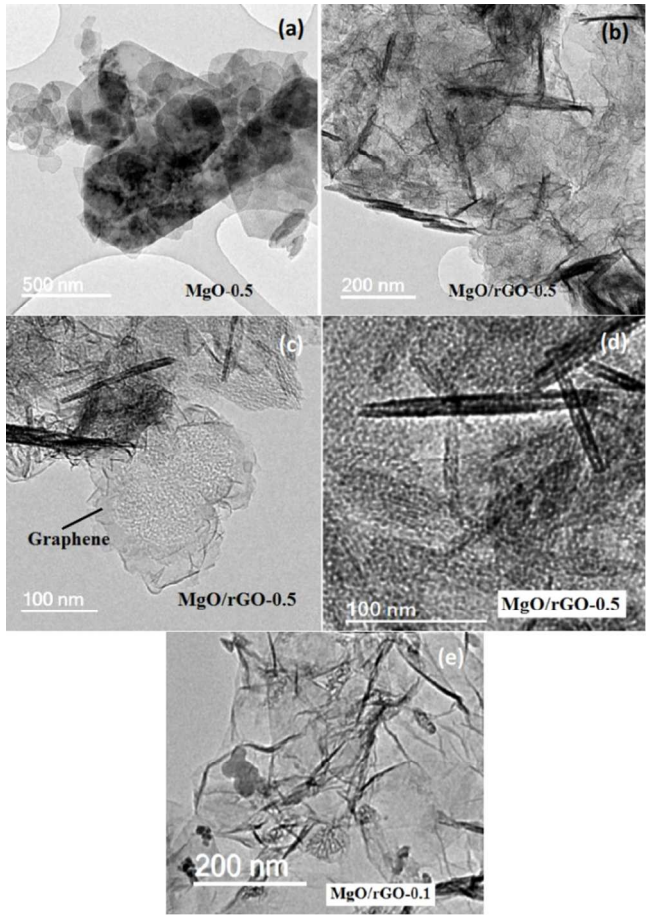

Figure 7. TEM images of MgO-0.5 in (a), MgO/rGO-0.5 in (b,c,d), and MgO/rGO-0.1 in (e).

Formation schemes of MgO in different morphologies on γ-Al_2O_3 and rGO

The formation of the different morphologies of MgO in this work was dependent on the use of confinement substrate. When using a substrate, MgO tended to follow the morphology of the substrate. Figure 8 sketches the simplified formation schemes of the MgO in different morphologies on γ-Al_2O_3 and rGO according to the obtained experimental results. Typical TEM image of the obtained MgO from each route was also inserted, relating the experimental results to the theoretical predictions.

When using aluminium tri-sec-buoxide and magnesium nitrate with a sol-gel method, a molecular network containing Al, Mg and O was formed after hydrolysis and condensation reactions in sol-gel chemistry. The γ-Al_2O_3 formed in this route was of high surface area and nano-sized particles known from a previous study[16]. Therefore upon calcining MgO nucleated together with γ-Al_2O_3, however its crystal growth was largely restricted by the γ-Al_2O_3 crystals, leading to fully mixed spherical nanocrystallites of MgO and γ-Al_2O_3, as substantiated by the inserted TEM image (a) and Figure 3.

On the other hand, the formation scheme of using $Mg(NO_3)_2$, GO and NH_4OH in precursor with a hydrothermal process was illustrated as comparison. As drawn from the experimental results, when using 1 g $Mg(NO_3)_2$ in the precursor, $Mg(OH)_2$ crystals nucleated on rGO. Its crystal growth was restricted by the neighbouring MgO crystals, leading to a full coverage on the rGO sheets with nanosized $Mg(OH)_2$ crystals. The bare rGO sheets were hardly observed under TEM. Because of the excessive amount of the $Mg(NO_3)_2$ in precursor, $Mg(OH)_2$ also nucleated outside of the rGO sheets and further grew into nanowhiskers, resulted from crystal growth along z axis for hexagonal lattice. Upon calcining, $Mg(OH)_2$ transformed to MgO but the morphologies remained, which is typical when converting hydroxides to oxides[19]. Similarly, when using 0.5 g $Mg(NO_3)_2$, MgO nanocrystals were formed on rGO sheets together with the separately formed nanowhiskers. The amount of MgO formed was much less, also indicated from the lighter colour in the TEM image (c) than in (b). However, when further lowing the amount of $Mg(NO_3)_2$ to 0.1 g, MgO whiskers were not observed and all the formed MgO particles were attached on the rGO sheets, as shown in the inserted TEM image (d). This proved that the $Mg(OH)_2$ preferred to nucleate on GO sheets first due to the oxygen bond. When the oxygen bond was fully occupied, $Mg(OH)_2$ started to nucleate separately outside of the GO sheets to further grow into nanowhiskers, as in the cases of using 1g and 0.5 g $Mg(NO_3)_2$ in precursor.

CO_2 uptake of MgO/ γ-Al_2O_3 and MgO/rGO

Table 1. Summary of the characterization results of the different samples.

Samples	S_{ssa} (m^2/g)	Pore size (nm)	CO_2 capture (mg/g)	Morphology
MgO	80	At around 5 nm	< 5	-
M1.72A1	179	At around 20 nm	35	-
M0.86A1	283	At 2-3, and 30 nm	62	Spherical particles of 10 nm
M0.43A1	246	At 2-3, and 20 nm	129	-
MgO-0.5	136	At 4, and 100 nm	< 5	Hexagonal/spherical particles of 100-300nm, and rods of 1 micron length
MgO/rGO-0.5	191	At 2, and 100 nm	-	Sheets of microns, nano whiskers of 500 nm long
MgO-1	108	At 2-3, and 100 nm	< 5	Hexagonal/ spherical particles of 100-300nm
MgO/rGO-1	170	At 2-3, and 100 nm	15	Sheets of microns, nano whiskers and double layer packed whiskers of 500 nm

The CO_2 uptake of MgO/γ-Al_2O_3 and MgO/rGO is summarized in table 1, together with other information from the samples. For the pure MgO obtained by sol-gel method, the CO_2 uptake was very low, less than 5 mg/g, while the CO_2 uptake of the MgO/γ-Al_2O_3 composite was largely increased, i.e. to 129 mg/g for M0.43A1. The significant increase was expected from the increased surface area and decreased weight of MgO in the composite. For the approach of using GO as confinement substrate, the pure MgO samples, MgO-0.5 and MgO-1 also had very low CO_2 uptake of less than 5 mg/g. The CO_2 uptake of MgO/rGO-1 at 400 °C was tripled to 15 mg/g. The increase was not as significant as in the MgO/Al_2O_3 samples, which were possibly related to the morphology of the MgO as the surface

area of MgO/rGO-1 is nearly the same with M1.72A1. It would be helpful to also compare with the CO_2 uptake of the MgO/rGO-0.5 sample, however, we were not able to successfully measure the CO_2 uptake of MgO/rGO-0.5, due to the low density of the sample. For low density material, it was very difficult to fill 10 mg to the TG crucible and typically 10 mg was required to have reliable results.

Conclusions

Two synthesis approaches using γ-Al_2O_3 and GO were designed and applied to confine the crystal growth of MgO in order to enlarge its surface area. The CO_2 uptakes at 400 °C of the synthesized samples were improved compared with the pristine MgO. Use of γ-Al_2O_3 and GO also resulted in different morphologies of MgO. When using γ-Al_2O_3, spherical MgO particles were obtained and mixed with γ-Al_2O_3 particles. When using GO in the precursor, MgO grew on rGO sheets, together with MgO nanowhiskers. The nanowhisker of a double layer packed morphology was observed for the first time for MgO. This study clearly shows various substrates can affect the morphology of the confined MgO and the corresponding CO_2 uptake, giving insight to the future design of MgO based sorbents.

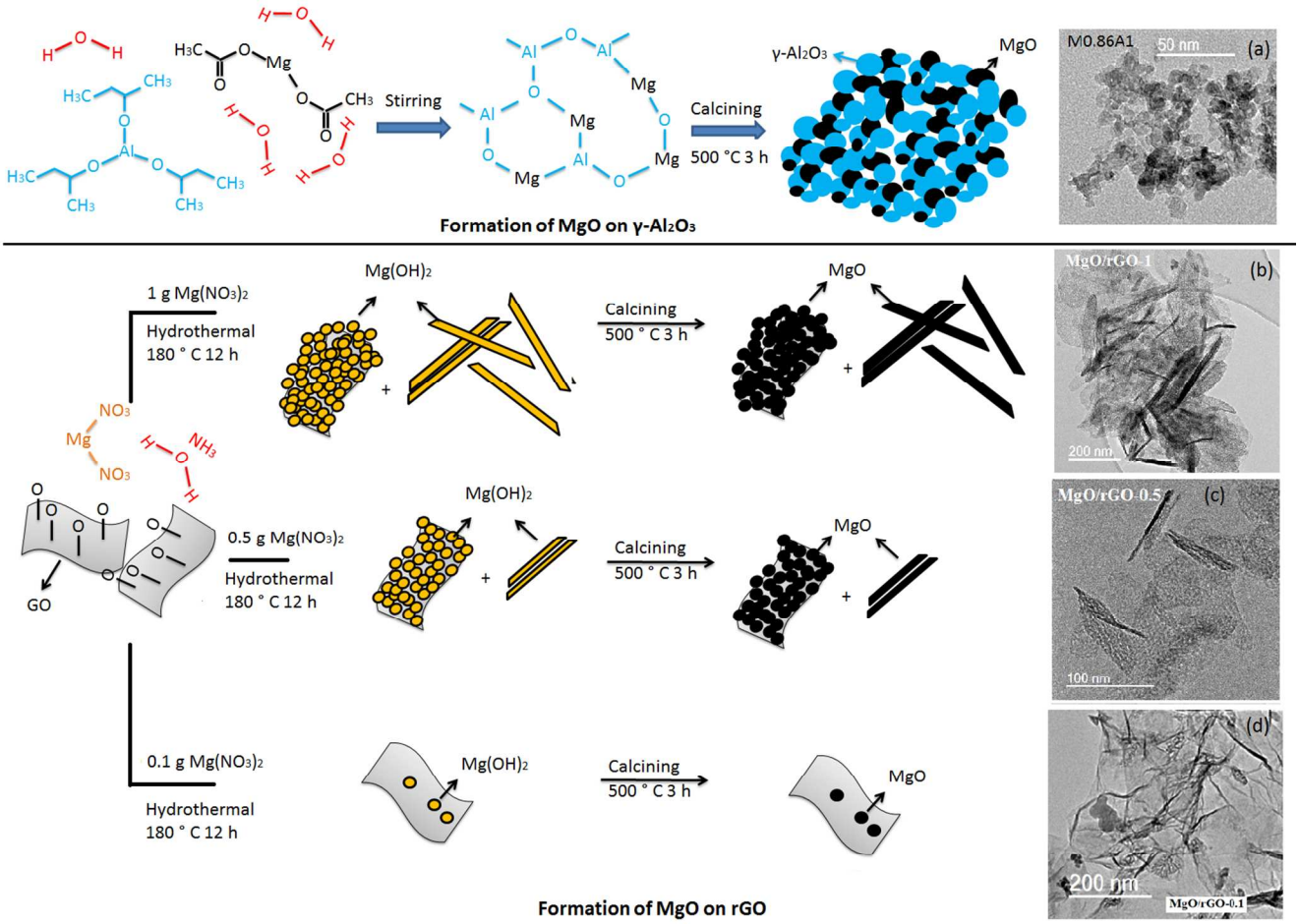

Figure 8. Schematic illustration of the formation schemes of the MgO in different morphologies on γ-Al_2O_3 and rGO. Observed TEM images from the relating samples are co-related after each route.

Notes and references

Corresponding author: z.x.guo@ucl.ac.uk

1 Bhagiyalakshmi, J. Lee, and H. Jang, Int. *J. Greenh. Gas Con.*, 4 (2010)51

2 M. Bhagiyalakshmi, P. Hemalatha, M. Ganesh, P. Mei, and H. Jang, *Fuel*, 90 (2011) 1662

3 Y. Li, K. Han, W. Lin, M. Wan, and Y. Wang, J. Zhu, *J. Mater. Chem. A*, 1 (2013) 12919

4 D. M. D'Alessandro, B. Smit, and J. R. Long, *Angew. Chem. Int. Ed*.49 (2010) 6058

5 A.H. Lu and G.P. Hao, *Annu. Rep. Prog. Chem., Sect. A: Inorg. Chem*. 109 (2013) 484

6 A. Samanta, A. Zhao, G. K. H. Shimizu, P. Sarkar and R. Gupta, *Ind. Eng. Chem. Res.* 51 (2012) 1438

7 F. Akhtar, Q. Liu, N. Hedin and L. Berqström, *Energy Environ. Sci*. 5 (2012) 7664

8 M. R. Mello, D. Phanon, G. Q. Silveria, P. L. Llewellyn and C. M. Ronconi, *Micropor. Mesopor. Mater.* 143 (2011) 174

9 M. G. Plaza, S. Garcia, F. Rubiera, J. J. Pis and C. Pevida, *Chem. Eng. J*, 163 (2010) 41

10 Z. Zhang, Y. Zhao, Q. Gong, Z. Li and J. Li, *Chem. Commun*. 49 (2013) 653

11 Q. Wang, J. Z. Luo, Z. Y. Zhong and A. Borgna, *Energy Environ. Sci.*

4 (2011) 42
[12] S. Wang, S. Yan, X. Ma and J. Gong, *Energy Environ. Sci*. 4 (2011) 3805
[13] J. V. Veselovskaya, V. S. Derevschikov, T. Y. Kardash, O. A. Stonkus, T. A. Trubitsina and A. G. Okunev, *Int. J. Greenh. Gas Con.* 17 (2013) 332
[14] X. Zhang, Y. Ge, S. P. Hannula, E. Levänen, T. Mäntylä, *J. Mater. Chem.* 19 (2009) 1915
[15] X. Zhang, Y. Ge, S. P. Hannula, E. Levänen, T. Mäntylä, *J. Mater. Chem.* 18 (2008) 2423
[16] X. Zhang, M. Honkanen, E. Levänen, T. Mäntylä, *J. Cryst. Growth* 310 (2008) 3674
[17] K. Qiu, Z. X. Guo, *J. Mater. Chem. A*. 2 (2014) 3209
[18] Y. Xu, K. Sheng, C. Li and G. Shi, *ACS Nano* 4 (2010) 4324
[19] X. Zhang, M. Honkanen, M. Järn, J. Peltonen, V. Pore, E. Levänen and T. Mäntylä, *App. Sur. Sci.* 254 (2008) 5129